JCI insight

Impaired PPARγ activation by cadmium exacerbates infection-induced lung injury

Jennifer L. Larson-Casey, … , David K. Crossman, A. Brent Carter

JCI Insight. 2023. https://doi.org/10.1172/jci.insight.166608.

Research In-Press Preview Infectious disease Pulmonology

Graphical abstract

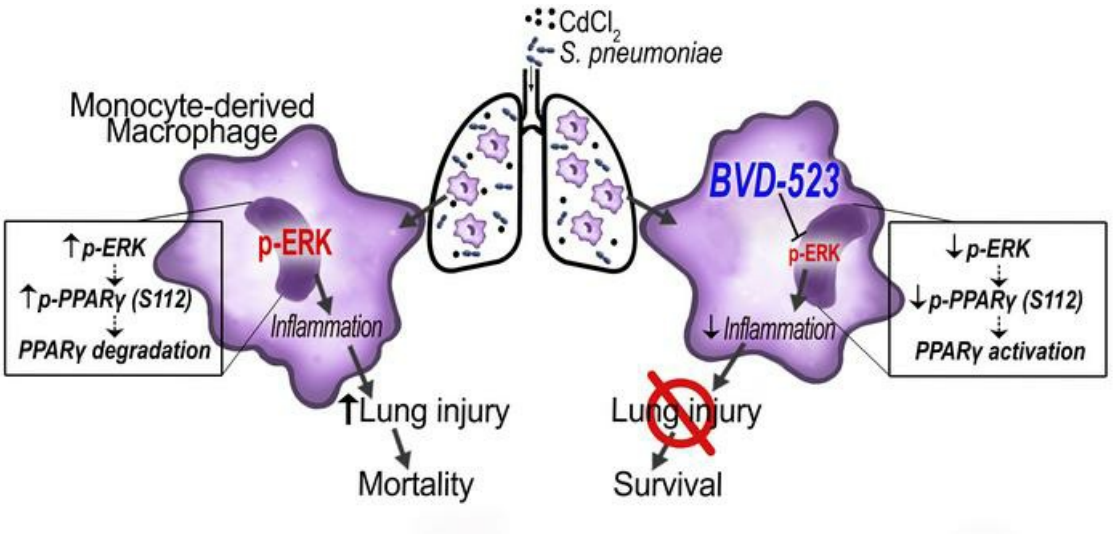

Impaired PPARγ activation by cadmium exacerbates infection-induced lung injury

Jennifer L. Larson-Casey[1,*], Shanrun Liu[2], Jennifer M. Pyles[3], Suzanne E. Lapi[3], Komal Saleem[1], Veena B. Antony[1], Manuel Lora Gonzalez[4], David K. Crossman[5], and A. Brent Carter[1,6,*]

[1]Department of Medicine, Division of Pulmonary, Allergy, and Critical Care Medicine, University of Alabama at Birmingham, Birmingham, AL, USA.
[2]Division of Clinical Immunology and Rheumatology, Department of Medicine, University of Alabama at Birmingham, Birmingham, Alabama.
[3]Department of Radiology, University of Alabama at Birmingham, Birmingham, AL.
[4]Department of Pathology, University of Alabama at Birmingham, Birmingham. AL, USA.
[5]Department of Genetics, University of Alabama at Birmingham, Birmingham, AL.
[6]Birmingham Veterans Administration Medical Center, Birmingham. AL, USA.
*To whom correspondence should be addressed: jennifercasey@uabmc.edu or bcarter1@uab.edu
[†]1918 University Blvd, 718 MCLM; Pulmonary, Allergy, and Critical Care Medicine, University of Alabama at Birmingham, Birmingham, AL 35294, USA. Tel. (205) 996-1683.

Abstract:

Emerging data indicates an association between environmental heavy metal exposure and lung disease, including lower respiratory tract infections (LRTIs). Here, we show by single cell RNA-sequencing an increase in *Pparg* gene expression in lung macrophages from mice exposed to cadmium and/or infected with *S. pneumoniae*. However, the heavy metal cadmium or infection mediated an inhibitory post-translational modification of peroxisome proliferator-activated receptor ɣ (PPARɣ) to exacerbate LRTIs. Cadmium and infection increased ERK activation to regulate PPARɣ degradation in monocyte-derived macrophages. Mice harboring a conditional deletion of *Pparg* in monocyte-derived macrophages had more severe *S. pneumoniae* infection after cadmium exposure, showed greater lung injury, and had increased mortality. Inhibition of ERK activation with BVD-523 protected mice from lung injury after cadmium exposure or infection. Moreover, subjects residing in areas of high air cadmium levels had increased cadmium concentration in their BAL fluid and showed PPARɣ inhibition that was mediated, at least in part, by ERK activation in isolated BAL cells. These observations suggest that impaired activation of PPARɣ in monocyte-derived macrophages exacerbates lung injury and the severity of LRTIs.

Introduction

Lower respiratory tract infections, including bacterial pneumonia, are a leading cause of adult morbidity and mortality in the United States and ranked fourth as the leading cause of death worldwide (1, 2). Approximately 120-156 million cases of lower respiratory tract infections (LRTIs) are reported annually worldwide leading to 1.4 million deaths (3). The primary infectious cause of respiratory failure is bacterial LRTI; in particular, *Streptococcus pneumoniae* is the leading cause of morbidity and mortality associated with LRTIs accounting for over 55% of LRTI deaths (3).

The adverse effects of air pollution are linked to many diseases, including cardiopulmonary disease, stroke, lung cancer, chronic respiratory disorders, and respiratory infections (4-6), and leads to substantial economic and healthcare costs (4). The component of air pollution containing particulate matter smaller than 2.5 μm in diameter ($PM_{2.5}$) has been identified as a potential contributor to respiratory infection in adults and children (7-9). Short-term increases in $PM_{2.5}$ are also associated with increased rates of hospitalizations secondary to respiratory infections (9, 10). Cadmium is enriched in $PM_{2.5}$ and has the capability to reach the alveolar space, which is particularly relevant in LRTIs (11). Widely distributed in the environment, natural air emission sources of cadmium can come from volcanoes, airborne soil particles, forest fires, coal fired plants, coke factories, and quarries (11). Cadmium adversely affects lung function and contributes to pulmonary fibrosis, cancer, asthma, and chronic obstructive pulmonary disease (12-14). Although environmental cadmium was recently identified to be associated with a higher risk of mortality from influenza or pneumonia (15), the mechanism(s) regulating cadmium-mediated respiratory infections is not known.

Lung macrophages play a critical role in host defense to respiratory pathogens (16). Bone marrow-derived monocytes are recruited to the lung during infection in a C-C-chemokine receptor type 2 (CCR2)-dependent manner (17). The increase in macrophage number seen in *S. pneumonia*-infected mice is due to macrophage recruitment, rather than expansion of the tissue resident alveolar macrophage population (18). Recruitment of monocyte-derived macrophages worsened *S. pneumoniae* infection in mice previously infected with influenza (19), which may be attributed to impaired efferocytosis and clearance of *S. pneumoniae* (20). Moreover, monocyte-derived macrophages contributed to enhanced inflammatory response and disease progression in several models of lung disease (21-26).

Our previous work showed that lung macrophages play a critical role in host defense to respiratory pathogens. Macrophage depletion significantly increased bacterial lung burden in mice, while no difference was detected in mice depleted of neutrophils (21). A recent study showed that cadmium-mediated lung injury resulted in the persistence of classically activated lung macrophages by inhibiting the nuclear localization of peroxisome proliferator-activated receptor ɣ (PPARɣ) (27). PPARɣ, a ligand activated transcription factor belonging to the nuclear receptor superfamily, is a negative regulator of the inflammatory response (28). PPARɣ is known to inhibit production of pro-inflammatory cytokines and reactive oxygen species generation. PPARɣ also controls the alternative activation of monocytes and macrophages (29).

PPARɣ contains a consensus mitogen-activated protein kinase (MAPK) site, and phosphorylation at serine 112 inhibits PPARɣ activation via degradation (30). The extracellular signal-regulated kinase (ERK) plays a pivotal role in lung inflammation (31) and has been implicated to be increased in mouse models of lung injury; however, the mechanism by which it contributes to lung injury has not been determined. We hypothesize that the heavy metal cadmium

regulated an inhibitory post-translational modification of PPARɣ to exacerbate LRTIs. Here, we show that recruited lung macrophages have a critical role in mounting an immune response to foreign agents to promote host defense but contribute to the pathogenesis of lung injury by impairment of PPARɣ activation via the activation of ERK. These observations suggest that PPARɣ is critical in regulating lung injury during LRTIs.

Results

Infection is exacerbated in mice exposed to cadmium.

Because cadmium is associated with increased risk of mortality from pneumonia (15), we questioned if cadmium altered the innate immune response to bacterial infections. Cadmium-exposed mice had increased number of BAL cells that increased further after exposure to *Streptococcus pneumoniae* (strain A66.1, type 3), as a model of LRTI (Figure 1A). Macrophages were the predominate cell type in the BAL fluid from cadmium-exposed and *S. pneumoniae*-infected mice throughout the duration after exposure. Neutrophils, however, only showed a transient increase after cadmium exposure and *S. pneumoniae* infection (Figure 1B, Supplemental Figure 1A-C). The lung from cadmium-exposed mice had thickened alveolar septa and cellular inflammation, and *S. pneumoniae* infected mice had similar findings as well as areas of consolidation (Figure 1C). The combination of cadmium and *S. pneumoniae* infection in mice had significantly greater consolidation with multi-lobar involvement. The histological findings were confirmed as cadmium-exposed mice had significantly greater lung colony-forming units than saline-exposed mice (Figure 1D). Moreover, cadmium-exposed mice had significantly greater mortality after infection (Figure 1E). These data indicate that cadmium exposure increases the severity of LRTI.

PPARγ is primarily expressed in macrophages.

To understand the cellular populations and mediators that increase the severity of LRTI, we performed single cell RNA-sequencing on unenriched single-cell suspensions from lung tissue of exposed mice. After quality filtering, we obtained 29,204 cell profiles from all samples.

Analysis of representative markers identified all major cell types within the mouse lung (Figure 2A).

Because PPARɣ plays a critical role in macrophage differentiation, we determined that *Pparg* was primarily expressed in macrophages (Figure 2B and Supplemental Figure 2A). Compared to all identified clusters, the robust expression of *Pparg* was maintained in macrophages in all exposure conditions (Figure 2C and Supplemental Figure 2B). Compared to the other identified isoforms of *Ppar*, *Pparg* showed the greatest expression in the macrophage cluster (Supplemental Figure 2C).

Cadmium mediated PPARɣ phosphorylation at Ser^{112} resulting in greater lung injury.

We questioned if cadmium regulated PPARɣ by altering the post-translational modification of PPARɣ. Cadmium exposure led to a marked increase in PPARɣ phosphorylation at its Ser^{112} residue, which correlated with the absence of PPARɣ nuclear localization; however, cadmium exposure did not lead to the phosphorylation of PPARɣ at its Ser^{273} residue (Figure 3 A, Supplemental Figure 3A-C). Similar results were obtained in BAL cells isolated from infected mice. Cadmium exposure mediated the phosphorylation of PPARɣ at Ser^{112} to a similar level seen in *S. pneumoniae*-infected mice (Figure 3B and Supplemental Figure 3D). Cadmium-exposed and *S. pneumoniae*-infected mice showed enhanced phosphorylation of PPARɣ at Ser^{112} and an absence of phosphorylation of PPARɣ at Ser^{273} and nuclear PPARɣ expression (Supplemental Figure 3E-F). Because phosphorylation can influence PPARɣ degradation (32), phosphorylation at Ser^{112} was linked to PPARɣ degradation as treatment with MG-132, a proteasome inhibitor, resulted in PPARɣ accumulation in the nucleus of cadmium-exposed macrophages (Figure 3C, Supplemental Figure 3G-I).

Validating that cadmium regulates the phosphorylation of PPARɣ at Ser^{112}, we mutated serine 112 to alanine ($PPAR\gamma_{S112A}$). Absence of PPARɣ (S112) phosphorylation in macrophages expressing the S112A mutant resulted in nuclear localization of PPARɣ in cadmium-exposed macrophages, whereas macrophages expressing $PPAR\gamma_{WT}$ showed increased p-PPARɣ (S112) expression and absent PPARɣ nuclear localization (Figure 3D, Supplemental Figure 3J-K). Confirming that cadmium mediated the degradation of PPARɣ via phosphorylation at Ser^{112}, cadmium-exposed macrophages expressing $PPAR\gamma_{WT}$ had increased p-PPARɣ (S112) expression; however, inhibiting degradation in the proteosome resulted in PPARɣ nuclear expression (Figure 3E, Supplemental Figure 3L-M). Macrophages expressing the mutant plasmid (S112A) maintained PPARɣ nuclear localization regardless of treatment with MG-132. The absence of nuclear PPARɣ expression was inversely correlated with p-PPARɣ (S112) expression in macrophages treated with cadmium (Figure 3F). Quantitatively determining the fraction of PPARɣ phosphorylated at Ser^{112} after cadmium exposure, lysates were subjected to PPARɣ immunoprecipitation. Cadmium-exposed macrophages showed increased p-PPARɣ (S112) expression with an absence in vehicle exposed, indicating nearly all of PPARɣ is phosphorylated at Ser^{112} after cadmium exposure (Figure 3G-H). Similar results were obtained in $PPAR\gamma_{WT}$-His transfected macrophages treated with cadmium (Supplemental Figure 3N).

To determine the physiologic role of cadmium and infection in the regulation in the post-translational modification of PPARɣ, we generated mice harboring a conditional deletion of *Pparg* in macrophages ($Pparg^{\Delta M}$). Cadmium-exposed or *S. pneumoniae*-infected $Pparg^{fl/fl}$ mice showed p-PPARɣ (S112) expression in the nuclear fraction of isolated lung macrophages (Figure 3I). Phosphorylation of PPARɣ at Ser^{112} was further increased in cadmium-exposed $Pparg^{fl/fl}$ mice after *S. pneumoniae* infection. $Pparg^{\Delta M}$ mice showed an absence of PPARɣ regardless of exposure. The

conditional deletion of *Pparg* did not alter normal lung architecture; however, $Pparg^{\Delta M}$ mice exposed to cadmium or infected with *S. pneumoniae* had greater cellular inflammation and consolidation. Essentially all the lung was consolidated in $Pparg^{\Delta M}$ mice exposed to cadmium followed by infection, whereas the $Pparg^{fl/fl}$ mice had partial consolidation (Figure 3J). The degree of lung inflammation and consolidation was quantified by scoring lung sections from both strains (Figure 3K-L). Interestingly, there was no difference in colony forming units in the lung between these strains of mice (Figure 3M); however, infected $Pparg^{\Delta M}$ mice had markedly reduced survival and a reduction in body weight (Figure 3N, Supplemental Figure 3O-P). Rather than increased bacterial burden, the increased mortality was associated with greater loss of barrier function and increased ratio of wet to dry lung weight, indicating more severe lung injury in the $Pparg^{\Delta M}$ mice (Figure 3O-P). These observations suggest that the severity of LRTI was secondary to increased lung injury via the impaired activation of PPARɣ.

ERK activation mediates phosphorylation of PPARɣ.

Mitogen-activated protein kinases (MAPK) regulate activation of multiple transcription factors (33), including the suppression of PPARɣ transcriptional activity by phosphorylation at Ser^{112} (34). Because cadmium was shown to augment NF-κB activity that resulted in the persistence of a pro-inflammatory phenotype in lung macrophages (27), we investigated if the extracellular signal-related kinase (ERK) was activated, as ERK is an essential regulator of NF-κB activity (33, 35). While cadmium increased ERK activity, cadmium-mediated ERK activation was inhibited in macrophages treated with a MEK inhibitor, U0126 (Figure 4 A-B), or macrophages expressing a dominant negative ERK (ERK_{DN}) (Figure 4D-E). ERK inhibition induced PPARɣ nuclear localization and inhibited phosphorylation of PPARɣ (S112) (Figure 4 C,

F, Supplemental Figure 4 A-B). Macrophages expressing constitutive active MEK1 showed ERK activation that increased further after cadmium exposure (Figure 4G-H). Constitutively active MEK1 alone or when combined with cadmium exposure led to PPARɣ inhibition with increased p-PPARɣ (S112) expression, whereas phosphorylation at the Ser^{273} residue was not altered (Figure 4I, Supplemental Figure 4C-D). These findings were specific to cadmium as other metals in particulate matter, such as arsenic or manganese, did not inhibit PPARɣ nuclear localization or alter phosphorylation at Ser^{112} via ERK activation (Supplemental Figure 4E). Visually confirming these results, vehicle-exposed macrophages had an absence of ERK activation, nuclear localization of PPARɣ, and absence of PPARɣ (S112) phosphorylation, whereas cadmium-mediated ERK activation and p-PPARɣ (S112) expression that caused retention of PPARɣ in the cytoplasm (Figure 4J-L, Supplemental Figure 4F).

To further investigate regulation of PPARɣ, single cell RNA-sequencing in lung tissue from exposed mice showed high expression of *Mapk1* in the macrophage cell cluster under all exposure conditions (Figure 4M and Supplemental Figure 3G-H). Validating these results, FACS-sorted BAL cells were subjected to immunoblot analysis. Cadmium exposure and *S. pneumoniae* infection mediated ERK activation and phosphorylation of PPARɣ (S112) only in monocyte-derived macrophages (MDMs) (Figure 4N and Supplemental Figure 4I). PPARɣ nuclear expression was detected in the tissue resident alveolar macrophages (TRAMs) and MDMs in saline exposed mice. MDMs from exposed or infected mice showed an absence of PPARɣ nuclear localization, whereas nuclear expression of PPARɣ was retained in TRAMs. To determine if PPARɣ was functionally active in TRAMs, we measured gene expression of arginase 1 (Arg1) as PPARγ binds to its promoter to induce transcription (29). PPARɣ-dependent Arg1 gene expression was minimally expressed in TRAMs from cadmium-exposed mice infected with *S. pneumoniae*

and remained at the same level regardless of the exposure condition (Supplemental Figure 4J). Taken together, these data show that monocyte-derived macrophage activation was regulated by ERK-mediated phosphorylation of PPARɣ at Ser^{112}.

Severe LRTIs inhibit PPARɣ expression in monocyte-derived macrophages.

Because our data implicates that cadmium regulates PPARɣ expression in monocyte-derived macrophages and is associated with more severe LRTIs, we further investigated the role of macrophage recruitment to the lung. Cadmium exposure and *S. pneumoniae* infection significantly increased MDMs in $Pparg^{fl/fl}$ and $Pparg^{\Delta M}$ mice (Figure 5A and C). $Pparg^{\Delta M}$ mice infected with *S. pneumoniae* after cadmium exposure showed significantly more MDMs than seen in $Pparg^{fl/fl}$ mice. In contrast, the number of TRAMs remained unchanged between strains and exposures (Figure 5A and B). The recruitment of MDMs correlated with increased TNF-α levels in the BAL fluid, and $Pparg^{\Delta M}$ mice showed greater levels after cadmium and infection than $Pparg^{fl/fl}$ mice (Figure 5D). IL-6, which has been associated with greater mortality, was increased in infected mice, and was markedly greater in $Pparg^{\Delta M}$ mice previously exposed to cadmium (Figure 5E). Because PPARɣ has been shown to regulate IL-10 production during bacterial infection (36, 37), we found that cadmium exposure and *S. pneumoniae* infection reduced IL-10 levels in the $Ppar^{fl/fl}$ mice, and the $Pparg^{\Delta M}$ mice showed an even greater reduction (Figure 5F). Validating that monocyte-derived macrophages are responsible for the inflammatory response to cadmium exposure, $CCR2^{-/-}$ mice showed a significant reduction in the inflammatory mediators, TNF-α and iNOS, compared to cadmium-exposed WT mice (Supplemental Figure 5A-D).

To further confirm the role of PPARɣ in MDMs, FACS-sorted BAL cells were subjected to confocal microscopy. PPARɣ was expressed in TRAMs from both strains regardless of exposure

(Figure 5G, Supplemental Figure 5E). MDMs from *Pparg*$^{fl/fl}$ mice showed ERK activation and PPARɣ (S112) phosphorylation after cadmium exposure or infection (Figure 5H-I). Although MDMs from *Pparg*$^{\Delta M}$ mice did not express PPARɣ or p-PPARɣ (S112), cadmium and *S. pneumoniae* infection induced ERK activation. Moreover, the absence of PPARɣ expression in MDMs from exposed mice was associated with markedly reduced IL-10 expression, whereas TRAMs showed no change in IL-10 (Figure 5J). These data suggest that the exacerbated lung injury in LRTIs is, in part, due to ERK activation in monocyte-derived macrophages.

Subjects residing in areas with high air cadmium levels show PPARɣ inhibition.

Neighborhoods surrounding industrial complexes have increased health risks from the continuous exposure to hazardous compounds released during active industrial activity . We obtained BAL from subjects residing in an area with a significant industrial legacy as well as continuous active industry, including coal fired plants, coke factories, and quarries. Compared to subjects from a control area where industrial activity was not present, subjects residing near the active industry had increased levels of cadmium in their BAL fluid (Figure 6A). The increased cadmium levels were associated with a loss of epithelial barrier function (Figure 6B). BAL cells isolated from cadmium-exposed subjects showed absence of PPARɣ localization in the nucleus, while PPARα and PPARδ isoforms were not altered (Figure 6C). Furthermore, ERK activation and phosphorylation of PPARɣ at Ser^{112} was present in cadmium-exposed subjects, but it was absent in control subjects. Cadmium-exposed subjects did not show p-38 or JNK activation, and phosphorylation of PPARɣ at Ser^{273} was not detected. TNF-α, IL-6, and IL-8 were significantly increased in the BAL fluid from cadmium-exposed subjects (Figure 6 D-G); however, IL-10 levels

were reduced, suggesting that the cadmium-exposed subjects have a pro-inflammatory state in their lung at baseline.

Inhibition of ERK reduces lung injury facilitating PPARg activation during LRTI.

To investigate the requirement of ERK activation mediating lung injury, we used BVD-523, an inhibitor of ERK activation. BVD-523, a small-molecule ERK1/2 kinase inhibitor, is currently under investigation in Phase 2 clinical trials for cancer therapy (38). Its effect in altering lung injury is not known. WT mice were exposed to saline or cadmium and infected with *S. pneumoniae.* Mice were administered vehicle or BVD-523 twice daily the day after infection. There was no difference in the BAL cell differential with the majority being a monocytic cell type (Supplemental Figure 5A). BVD-523 did not induce apoptosis, suggesting it was not toxic (Supplemental Figure 5B). BVD-523 inhibited ERK activation in cadmium-exposed or infected mice; however, BVD-523 did not alter p-38 and JNK activation by in mice (Figure 7A). PPARɣ phosphorylation at Ser^{112} was absent in isolated lung macrophages from mice treated with BVD-523, and BVD-523 did not alter phosphorylation at Ser^{273}. Furthermore, the treatment of mice with BVD-523 also rescued nuclear localization of PPARɣ in lung macrophages regardless of exposure.

BVD-523 did not alter normal lung architecture in saline-exposed mice (Figure 7C). Mice receiving vehicle showed cellular inflammation and consolidation after exposure to cadmium or infection with *S. pneumoniae*. Administration of BVD-523 did not alter consolidation or colony forming units in the lung (Figure 7C); however, compared to mice administered vehicle, mice receiving BVD-523 showed increased survival, increased barrier function, and reduced ratio of wet to dry lung weight, suggesting a reduction in lung injury (Figure 7D-F). The reduced lung injury in LRTI correlated with reduced TNF-α and IL-6 levels in mice treated with BVD-523

(Figure 7G and 7H). Moreover, IL-10 levels were increased in mice receiving BVD-523 (Figure 7I). In aggregate, these observations uncover a molecular mechanism by which cadmium exacerbates LRTIs and lung injury. These findings further suggest that inhibiting ERK activation in monocyte-derived macrophages to recover PPARɣ activation may be a novel therapeutic modality to lessen the severity of infection and lung injury in subjects living in areas with high levels of cadmium.

Discussion

Although lung injury after respiratory infection is often unavoidable, identifying modifiable risk factors that predispose individuals to severe pneumonia is an unmet need. Epidemiological studies have provided evidence on the adverse effects of exposure to airborne particles. Exposure to fine particulate matter ($PM_{2.5}$) is associated with increased rates of lung function decline, mortality, and respiratory morbidity (5, 6, 39-41). Recent data indicate that $PM_{2.5}$-associated deaths within the United States greatly affects individuals living in communities with greater socioeconomic deprivation, as well as non-Hispanic Black or African American individuals (42). Although the composition of $PM_{2.5}$ was not determined in this study, $PM_{2.5}$ is enriched with the heavy metal cadmium (43, 44), and exposure to cadmium has been shown to double the risk of lung disease (13). Here, we show that prior exposure to cadmium exacerbates lower respiratory tract infections (LRTIs) by enhancing the degradation of PPARɣ within specific lung macrophage subsets.

Monocyte-derived macrophages (MDMs) contribute to lung injury and lung remodeling by increased recruitment to the lung (27, 45, 46). The persistence of these cells within the lung months after initial injury may exacerbate lung injury and contribute to lasting health consequences, in part due to the robust pro-inflammatory response of recruited MDMs. Evidence suggests that tissue resident alveolar macrophages (TRAMs) and MDMs respond differently to lung injury (47). The number of MDMs in the lung may contribute to exacerbated inflammatory responses and disease severity, which was recently identified in COVID-19 patients (26).

Peroxisome proliferator-activated receptor ɣ (PPARɣ), a ligand activated nuclear receptor, is a negative regulator of the inflammatory response by inhibiting production of pro-inflammatory cytokines, including TNF-α and IL-6 (28). PPARɣ activation opposes inflammation in

macrophages most notably by inhibiting inflammatory transcription factors, such as NF-κB and AP-1, and increases expression of IL-10 (29). Controversy exists on the role of PPARɣ in bacterial infections. Conditional deletion of PPARɣ in myeloid cells in mice showed a hyperinflammatory response to infections to promote pathogen clearance in response to *Mycobacterium tuberculosis, Salmonella Typhimurium, Brucella abortus,* and *Listeria monocytogenes* infection (48-50).

Phosphorylation of PPARɣ at Ser^{112} was recently shown to be mediated by the upstream c-Jun N-terminal kinase-mitogen-activated protein kinase (JNK-MAPK) in a murine acute lung injury model (36). Although cadmium exposure promoted JNK activation, our data demonstrate that ERK activation was, at least in part, responsible for the increased lung injury seen in these mice, and ERK inhibition did not alter JNK activation. ERK has also been shown to phosphorylate PPARɣ at Ser^{273} and Ser^{133} (51). Phosphorylation at Ser^{273} is linked with the development of insulin resistance in mice; however, PPARɣ protein degradation has not been associated with phoshorylation at these sites and cadmium did not promote phosphorylation of PPARɣ at Ser^{273}.

Selective ERK inhibitors have been used in clinical trials for the treatment of a variety of cancers. These compounds either disrupt ERK dimerization or bind to the active conformation site to inhibit kinase activity and phosphorylation of downstream kinases. BVD-523, the most advanced ERK inhibitor currently in phase I/II trial, showed ERK inhibition in whole blood from enrolled subjects and preliminary efficacy in patients with advanced solid tumors (38). ERK activation has been shown to be increased in mouse models of acute lung injury (52); however the mechanism by which its inhibition contributes to lung injury has not been determined. Data here indicated ERK inhibition attenuates phosphorylation of PPARɣ at Ser^{112} to maintain nuclear PPARɣ expression and activation. Furthermore, administration of BVD-523 in cadmium-exposed or infected mice abrogated lung injury.

The thiazolidinedione class of PPARɣ agonists, including rosiglitizone and pioglitazone, are used in the treatment of type 2 diabetes by improving insulin sensitivity. Administration of the PPARɣ agonist, rosiglitazone, has been shown to promote the transition from the inflammatory phase to resolution and enhanced clearance of *S. aureus* in mice (53). Although these agonists were beneficial in promoting insulin-sensitization, these drugs are associated with many adverse effects, including weight gain, fluid retention, congestive heart failure, and bone fractures (54). This evidence indicated that alternative strategies for targeting PPARɣ are warranted. Data presented here identifies that ERK regulates the phosphorylation of PPARɣ at Ser^{112} to promote degradation of the protein. We have identified that targeting this post-translational modification of PPARɣ in monocyte-derived macrophages may be a promising therapeutic target.

The induction of TNF-α in response to LPS has been shown to require ERK activation and the ERK pathway is essential for the transcriptional regulation of TNF-α (55). Our data support these observations. Cadmium-exposed subjects had increased levels of TNF-α in the BAL fluid. This is especially interesting in that these subjects also showed ERK activation in isolated lung macrophages. TNF-α plays an essential role in inflammation and immune homeostasis (56), but it has been implicated in many of the detrimental effects of chronic inflammation. Increased plasma levels of soluble TNF receptors are strongly associated with mortality and morbidity in patients with acute lung injury (57). Our data shows that reduced lung injury is associated with reduced inflammation.

Our study has several limitations. Our single cell RNA sequencing analysis was able to capture many cell types within the lung; however, we were not able to resolve tissue resident and monocyte-derived macrophage subsets in exposed mice. Although interstitial macrophages showed limited expression for *Pparg* in exposed mice, we did not evaluate the contribution of

these cells, as evidence suggests that monocytes give rise to interstitial macrophages and then differentiate into monocyte-derived macrophages. Another limitation is the composition of $PM_{2.5}$ was not determined in this study. Because $PM_{2.5}$ may contain various heavy metals, it is possible that other metals could share this mechanism. Additionally, the cadmium-exposed subjects recruited for this study had no recent or current evidence of infection, follow-up studies should assess the subject's history of LRTIs. In aggregate, these observations suggest that the regulation of PPARɣ in monocyte-derived macrophages is novel target to protect against the severity of LRTIs secondary to lung injury mediated by air pollution.

Methods

Human subjects. We obtained human BAL cells from normal subjects and subjects from an area with high air cadmium levels under approved protocols (300004607 and 300001124) by the Human Subjects Institutional Review Boards of UAB. Human BAL specimens were used for research only. All subjects provided prior written consent to participate in the study. Normal volunteers had to meet the following criteria: 1) age between 18 and 75 years; 2) no history of cardiopulmonary disease or other chronic disease; 3) no prescription or nonprescription medication except oral contraceptives; 4) no recent or current evidence of infection; and 5) lifetime nonsmoker (< 5 packs in lifetime). Cadmium-exposed subjects had to meet the following criteria: 1) resident from the Affected and Control Areas (zip codes 35207, 35217, and 35214) in North Birmingham, Alabama who have lived at these sites for a minimum of 2 years; 2) FEV1 (forced expiratory volume in one second) greater than one liter; 3) oxygen saturation greater than 90% at rest on room air; 4) current nonsmoker; 5) no recent or current evidence of infection. Fiberoptic bronchoscopy with bronchoalveolar lavage was performed after subjects received local anesthesia. Three sub-segments of the lung were lavaged (right middle lobe, right upper lobe, and lingual) with five 20-ml aliquots of normal saline, and the first aliquot in each was discarded. The percentage of macrophages was determined by Wright-Giemsa stain and varied from 90 to 98%.

Mice. Animal experiments were approved by UAB Institutional Animal Care and Use Committee under protocols 21969 and 21149 and were performed in accordance with NIH guidelines. WT C57BL/6J and *CCR2*$^{-/-}$ mice were purchased from JAX Labs. *Pparg*$^{fl/fl}$ mice (a generous gift from Troy Randall, University of Alabama at Birmingham) were bred with mice containing a Cre recombinase under the control of the lysozyme M promoter. The resulting *Pparg*$^{-/-}$*Lyz2-cre* mice (referred to herein as *Pparg*$^{\Delta M}$*)* were generated by selective disruption of *Pparg* in

the cells of the granulocyte/monocyte lineage as previously described (58). *Pparg*$^{fl/fl}$ mice were used as controls unless otherwise noted. 8- to 12-week-old male and female mice were intratracheally administered 100 ng/kg of $CdCl_2$ or saline, as a vehicle control, after being anesthetized with 3% isoflurane using a precision Fortec vaporizer. This dose was the determined cadmium concentration in BALF from mice exposed to cigarette smoke measured by Inductively Coupled Plasma Mass Spectrometry (ICP-MS) (21). For in vivo bacterial infection studies, mice were administered sterile saline or 10^3 *Streptococcus pneumoniae* (strain A66.1, type 3) i.t and were euthanized after 15 days. Bacterial infections were performed 5 days after cadmium exposure. Mice were monitored every 4-6 hours after bacterial exposure for the duration of the exposure. BVD-523 (8.6 mg/kg, Selleck) was administered twice daily by oral gavage 1 day after S. *pneumoniae* infection until day 15. Dosing in mice was equivalent to the 600 mg dose used in phase 2 clinical trial (NCT04488003). Whole lung lavage was conducted and cytospins were generated to determine cell differential by Wright-Giemsa stain.

Cell culture. Human monocyte (THP-1) and mouse alveolar macrophage (MH-S) cell lines were obtained from American Type Culture Collection. Macrophages were maintained in RPMI 1640 media with 10% fetal bovine serum and penicillin/streptomycin supplements. All experiments were conducted in RPMI containing 0.5% serum. Cells were treated with the MAPK/ERK kinase (MEK) inhibitor, U0126 (10 μM, 1 h), prior to cadmium exposure. Cells were treated with vehicle or 50 μM $CdCl_2$ for 3 h or indicated time as previously described (27).

Quantitative real time PCR. Total RNA was isolated, reverse transcribe, and quantitative real-time PCR was performed as described previously (58). Data was calculated by the cycle threshold ($^{\Delta\Delta}$CT) method, normalized to β-actin, and expressed in arbitrary units. The following

primer sets were used: mouse arginase 1: 5'-CAG AAG AAT GGA AGA GTC AG-3' and 5'-CAG ATA TGC AGG GAG TCA CC-3'.

Plasmids and transfection assays. The pCMV-MEK1 and pCMV-HA-ERK2 (K/A) (ERK_{DN}) plasmids (generous gifts from Dr. Roger Davis, University of Massachusetts) have been previously described (33). Mouse PPARɣ plasmid, a gift from Dr. Bruce Spiegelman, was purchased from Addgene #8895 (32). Site directed mutation of PPARɣ (S112A) was performed using the Q5® Site-Directed Mutagenesis Kit (BioLabs# E0552S). The correct reading frame and sequence was verified by the Heflin Center Genomics Core at UAB. Cells were transfected using X-treme GENE 9 Transfection Reagent (Roche Applied Scientific) according to the manufacturer's protocol.

Flow cytometry. BAL cells were blocked with 1% BSA containing TruStain fcX (anti-mouse CD16/32) antibody (101319; BioLegend), followed by staining with antibodies. Antibodies used: Rat anti-mouse CD45-PE (12-0451-82; eBiosciences), LIVE Dead-eflour506 (65-0866; Invitrogen), Rat anti-mouse CD11b-APC-Cy7 (101225; BioLegend), anti-mouse CD64-PE-Cy7 (139313; BioLegend), Rat anti-mouse Ly6G-AF700 (561236; BD), Rat anti-mouse Siglec F-APC (155507; BioLegend), Rat anti-mouse Ly6C: eflour450 (48-5932-82; Invitrogen), Rat anti-mouse MHC II-PerCP-Cy5.5 (562363; BD). Hierarchical gating strategy was used to represent the tissue resident alveolar macrophages as $CD45^{+}CD11b^{+/-}Ly6G^{-}CD64^{+}Ly6C^{-}$Siglec F^{hi} and monocyte-derived macrophages as $CD45^{+}CD11b^{+/-}Ly6G^{-}CD64^{+}Ly6C^{-}$Siglec F^{low}. Data was acquired on FACSAria II or LSR II (BD Biosciences) using BD FACS DIVA software (version 8.0.1). Data were analyzed using FlowJo (FlowJo LLC) software (Version 10.5.0).

Single cell RNA sequencing. Single cell suspensions were prepared as previously described (45) with slight modification. Lungs were perfused with 10 mL HBSS, removed, and infused with

1 ml digestion solution (dispase with 0.2 mg/ml DNase I). Lungs were incubated at room temperature for 45 min with gentle agitation and tissue was gently teased apart with forceps into 1-2 mm fragments and incubated in digestion buffer for 15 min. Solution was filtered through a 70 μm cell strainer, washed with DMEM containing 5% FBS, centrifuged, and RBCs lysed with ACK lysing buffer. Resulting single cell suspension was filtered twice through a 40 μm cell strainer with DMEM containing 5% FBS. Cells were counted after staining with 7-AAD for exclusion of nonviable cells, cell viability exceeded 95%.

The 10X Genomics Cellranger software (version 7.0.0), mkfastq, was used to create the fastq files from the sequencer. After fastq file generation, Cellranger count was used to align the raw sequence reads to the mouse reference genome (mm10). The matrix tables created by count was then loaded into the R package Seurat (version 4.1.1) which allows for selection and filtration of cells based on quality control metrics, data normalization and scaling, and detection of highly variable genes (59). The Seurat vignette (https://satijalab.org/seurat/articles/pbmc3k_tutorial.html) was followed to create the Seurat data matrix object. In brief, we kept all genes expressed in more than three cells and cells with at least 200 detected genes. Cells with mitochondrial gene percentages >10% and unique gene counts > 6000 or < 200 were discarded. The data were normalized using Seurat's NormalizeData function, which uses a global-scaling normalization method, LogNormalize, to normalize the gene expression measurements for each cell to the total gene expression. The result is multiplied by a scale factor of 1e4 and the result is log-transformed. Highly variable genes were then identified using the function FindVariableFeatures in Seurat. SelectIntegrationFeatures was used to select features that are repeatedly variable across the samples for integration. Anchors were identified using FindIntegrationAnchors which takes the above integration features. These anchors were then

used to integrate the samples together with IntegrateData. Variation was regressed arising from library size and percentage of mitochondrial genes using the Seurat function ScaleData. PCA was performed of the variable genes as input and determined significant principal components on the basis of the Seurat JackStraw function. The first 30 principal components were selected as input for UMAP using FindNeighbors, FindClusters (resolution = 0.8) and RunUMAP in Seurat. To help aid in identifying cell types, SingleR (version 1.10.0) was used to annotate the identified clusters and manually verified with FindConservedMarkers (46). To identify differentially expressed genes (DEGs) in each cell cluster, we used Seurat's FindMarkers function on normalized gene expression.

Confocal imaging. Macrophages and BAL cells were fixed with 4% paraformaldehyde in PBS for 45 min at room temperature, followed by permeabilization for 3 min and incubated with PBS containing 5% BSA for 45 min. Cells were incubated with PPARɣ anti-rabbit (A0270; Abclonal), phospho-PPARɣ anti-rabbit (04-816-I; Sigma), or phospho-ERK anti-mouse (675502; Biolegend) and Goat Anti-Rabbit IgG-FITC (4030-02; Southern Biotech) or Goat Anti-Mouse IgG, Human ads-TRITC (1030-03; Southern Biotech) and counterstained with DAPI. Nikon A1 Confocal was utilized for imaging.

Inductively Coupled Plasma Mass Spectrometry (ICP-MS). Cd levels in BAL samples were measured using inductively coupled plasma mass spectrometry (ICP-MS 7500a, Agilent, USA). An aliquot (500 µL) was prepared as previously described (21). Samples were analyzed in sextuplicate, and the concentration was calculated using a standard calibration curve. All dilution solutions used for analysis were treated with Chelex 100 resin to remove cations.

Lung Bacterial Burden. Bacterial burden was determined in excised lungs as previously described (21). Lungs were homogenized in PBS and serial, 3-fold dilutions were made and plated

on blood agar plates containing 4 μg/ml gentamicin sulfate. The CFU's were determined ~16 h after plating and incubation; results were expressed as CFU per ml of lung tissue.

Isolation of nucleus. Nuclear isolation was performed by resuspending cells in a lysis buffer (10mM HEPES, 10mM KCL, 2mM $MgCl_2$, 2 mM EDTA) for 15 min on ice. Nonidet P-40 (10%) was added to lyse the cells, and the cells were centrifuged at 4 °C at14,000 rpm. The nuclear pellet was resuspended in an extraction buffer (50 mM HEPES, 50 mM KCL, 300 mM NaCl, 0.1 mM EDTA, 10% glycerol) for 20 min on ice. After centrifuging at 4 °C at 14,000 rpm, the supernatant was collected as nuclear extract (33).

Immunoblot analysis. Primary antibodies used: Lamin A/C (2032), Rabbit monoclonal anti-phospho-p38 MAPK (Thr180/Tyr182) (9215), phospho-SAPK/JNK (Thr183/Tyr185) (9255) (Cell Signaling); β-actin (A5441) and phospho-PPARɣ S112 (04-816-I) (Sigma); phospho-ERK (sc-7383) (Santa Cruz Biotechnology); PPARɣ (A0270) (Abclonal); PPARα (PAa-822A), PPARδ (PA1-823A); phospho-PPARɣ S273 (BS-4888R) (ThermoFisher Scientific).

Immunoprecipitation. Immunoprecipitation of PPARɣ was performed by lysing 10 million cells in buffer supplemented with EDTA-free protease inhibitor cocktail. Beads from Dynabeads Protein G Kit (Invitrogen, 10007D) were incubated with PPARɣ antibody (ProteinTech, 16643-1-AP) to form beads-antibody complex. To avoid co-elution of the bound antibody, the complex was crosslinked with disuccinimidyl suberate Equal amount of total protein from supernatant was incubated with the beads-antibody complex overnight at 4˚C. The complex was washed three times and eluted. Purification of His-tagged proteins was performed as previously described (21).

ELISA. IL-6, IL-8, and TNF-α expression were determined in BALF using ELISA kits (R&D Systems) according to the manufacturer's instructions.

Albumin. Albumin levels were determined in BAL fluid using the human (Millipore) or mouse Albumin ELISA Kit (Immunology Consultants Laboratory) according to the manufacturer's protocol. Samples were diluted 1/500,000.

Materials. U0126 and MG-132 were purchased from Sigma Chemical Company.

Statistics. Statistical comparisons were performed using a student's *t* test when only two groups of data are presented, or one-way ANOVA with a Tukey's *post hoc* test or and two-way ANOVA followed by Bonferroni post-test when multiple data groups are presents. All statistical analysis was expressed as ±S.E.M. and $p < 0.05$ was considered to be significant. GraphPad Prism statistical software was used for all analysis.

Data Availability. Data have been submitted to the National Center for Biotechnology Information (NCBI) Gene Expression Omnibus database (GEO) with GEO accession number GSE225386.

Statistical Analysis. Statistical comparisons were performed using a student's *t* test when only two groups of data are presented, or one-way ANOVA with a Tukey's post hoc test. All statistical analysis was expressed as ±S.E.M. and $p < 0.05$ was considered to be significant. GraphPad Prism statistical software was used for all analysis.

Study Approval. We obtained BAL cells under an approved protocol (300004607 and 300001124) by the Human Subjects Institutional Review Board of the University of Alabama at Birmingham. Human BAL specimens were used for research only. All subjects provided prior written consent to participate in the study. Animal experiments were approved by the University of Alabama at Birmingham Institutional Animal Care and Use Committee under protocols 21969 and 21149 and were performed in accordance with NIH guidelines.

Author Contributions: JLC and ABC developed the concept and design of the study. JLC, SL, and JMP assisted with conducting experiments. JLC, SL, JMP, SEL, DKC, KS, VBA, and ABC acquired data. JLC, SEL, VBA, and ABC provided reagents. JLC, JMP, SEL, DKC, MLG, and ABC provided analysis and interpretation of experiments and results. JLC and ABC wrote the manuscript.

Acknowledgments: We thank Dr. Linlin Gu, for assistance in generating the PPARɣ S112A mutant plasmid, Harish Chandra Pal and the Comprehensive Flow Cytometry Core for assistance with flow cytometry, and the generous gift from Dr. Roger Davis, University of Massachusetts, for providing the pCMV-MEK1 and pCMV-HA-ERK2(K/A) plasmids. Research reported in this publication was supported by the National Institute of Health grants 5R01ES015981-15, 5P01 HL114470-10, and P42 ES027723-03, and 5I01 CX001715-04 to the Department of Veteran Affairs to ABC, and a University of Alabama at Birmingham Faculty Development Grant to JLC. Support for the Comprehensive Flow Cytometry Core provided by the Center for AIDS Research, AI027767, The O'Neal Comprehensive Cancer Center, CA013148 and the UAB High Resolution Imaging Facility.

Competing Interests Statement: The authors declare no conflict of interest exists.

References and Notes

1. Diseases GBD, and Injuries C. Global burden of 369 diseases and injuries in 204 countries and territories, 1990-2019: a systematic analysis for the Global Burden of Disease Study 2019. *Lancet.* 2020;396(10258):1204-22.
2. Ahmad FB, and Anderson RN. The Leading Causes of Death in the US for 2020. *JAMA.* 2021;325(18):1829-30.
3. Collaborators GBDLRI. Estimates of the global, regional, and national morbidity, mortality, and aetiologies of lower respiratory infections in 195 countries, 1990-2016: a systematic analysis for the Global Burden of Disease Study 2016. *Lancet Infect Dis.* 2018;18(11):1191-210.
4. Landrigan PJ, Fuller R, Acosta NJR, Adeyi O, Arnold R, Basu NN, et al. The Lancet Commission on pollution and health. *Lancet.* 2018;391(10119):462-512.
5. Samet JM, Dominici F, Curriero FC, Coursac I, and Zeger SL. Fine particulate air pollution and mortality in 20 U.S. cities, 1987-1994. *N Engl J Med.* 2000;343(24):1742-9.
6. Liu C, Chen R, Sera F, Vicedo-Cabrera AM, Guo Y, Tong S, et al. Ambient Particulate Air Pollution and Daily Mortality in 652 Cities. *N Engl J Med.* 2019;381(8):705-15.
7. Cohen AJ, Brauer M, Burnett R, Anderson HR, Frostad J, Estep K, et al. Estimates and 25-year trends of the global burden of disease attributable to ambient air pollution: an analysis of data from the Global Burden of Diseases Study 2015. *Lancet.* 2017;389(10082):1907-18.
8. Horne BD, Joy EA, Hofmann MG, Gesteland PH, Cannon JB, Lefler JS, et al. Short-Term Elevation of Fine Particulate Matter Air Pollution and Acute Lower Respiratory Infection. *Am J Respir Crit Care Med.* 2018;198(6):759-66.
9. Croft DP, Zhang W, Lin S, Thurston SW, Hopke PK, Masiol M, et al. The Association between Respiratory Infection and Air Pollution in the Setting of Air Quality Policy and Economic Change. *Ann Am Thorac Soc.* 2019;16(3):321-30.
10. Krall JR, Mulholland JA, Russell AG, Balachandran S, Winquist A, Tolbert PE, et al. Associations between Source-Specific Fine Particulate Matter and Emergency Department Visits for Respiratory Disease in Four U.S. Cities. *Environ Health Perspect.* 2017;125(1):97-103.
11. Faroon O, Ashizawa A, Wright S, Tucker P, Jenkins K, Ingerman L, et al. *Toxicological Profile for Cadmium*. Atlanta (GA): Agency for Toxic Substances and Disease Registry (US); 2012.
12. Lampe BJ, Park SK, Robins T, Mukherjee B, Litonjua AA, Amarasiriwardena C, et al. Association between 24-hour urinary cadmium and pulmonary function among community-exposed men: the VA Normative Aging Study. *Environ Health Perspect.* 2008;116(9):1226-30.
13. Mannino DM, Holguin F, Greves HM, Savage-Brown A, Stock AL, and Jones RL. Urinary cadmium levels predict lower lung function in current and former smokers: data from the Third National Health and Nutrition Examination Survey. *Thorax.* 2004;59(3):194-8.
14. Li FJ, Surolia R, Singh P, Dsouza KG, Stephens CT, Wang Z, et al. Fibrinogen mediates cadmium-induced macrophage activation and serves as a predictor of cadmium exposure

in chronic obstructive pulmonary disease. *Am J Physiol Lung Cell Mol Physiol.* 2022;322(4):L593-L606.
15. Park SK, Sack C, Siren MJ, and Hu H. Environmental Cadmium and Mortality from Influenza and Pneumonia in U.S. Adults. *Environ Health Perspect.* 2020;128(12):127004.
16. Knapp S, Leemans JC, Florquin S, Branger J, Maris NA, Pater J, et al. Alveolar macrophages have a protective antiinflammatory role during murine pneumococcal pneumonia. *Am J Respir Crit Care Med.* 2003;167(2):171-9.
17. Serbina NV, and Pamer EG. Monocyte emigration from bone marrow during bacterial infection requires signals mediated by chemokine receptor CCR2. *Nat Immunol.* 2006;7(3):311-7.
18. Taut K, Winter C, Briles DE, Paton JC, Christman JW, Maus R, et al. Macrophage Turnover Kinetics in the Lungs of Mice Infected with Streptococcus pneumoniae. *Am J Respir Cell Mol Biol.* 2008;38(1):105-13.
19. Ellis GT, Davidson S, Crotta S, Branzk N, Papayannopoulos V, and Wack A. TRAIL+ monocytes and monocyte-related cells cause lung damage and thereby increase susceptibility to influenza-Streptococcus pneumoniae coinfection. *EMBO Rep.* 2015;16(9):1203-18.
20. Medeiros AI, Serezani CH, Lee SP, and Peters-Golden M. Efferocytosis impairs pulmonary macrophage and lung antibacterial function via PGE2/EP2 signaling. *J Exp Med.* 2009;206(1):61-8.
21. Larson-Casey JL, Gu L, Jackson PL, Briles DE, Hale JY, Blalock JE, et al. Macrophage Rac2 Is Required to Reduce the Severity of Cigarette Smoke-induced Pneumonia. *Am J Respir Crit Care Med.* 2018;198(10):1288-301.
22. Aegerter H, Kulikauskaite J, Crotta S, Patel H, Kelly G, Hessel EM, et al. Influenza-induced monocyte-derived alveolar macrophages confer prolonged antibacterial protection. *Nat Immunol.* 2020;21(2):145-57.
23. Pisu D, Huang L, Narang V, Theriault M, Le-Bury G, Lee B, et al. Single cell analysis of M. tuberculosis phenotype and macrophage lineages in the infected lung. *J Exp Med.* 2021;218(9).
24. Mould KJ, Jackson ND, Henson PM, Seibold M, and Janssen WJ. Single cell RNA sequencing identifies unique inflammatory airspace macrophage subsets. *JCI Insight.* 2019;4(5).
25. Li F, Piattini F, Pohlmeier L, Feng Q, Rehrauer H, and Kopf M. Monocyte-derived alveolar macrophages autonomously determine severe outcome of respiratory viral infection. *Sci Immunol.* 2022;7(73):eabj5761.
26. Szabo PA, Dogra P, Gray JI, Wells SB, Connors TJ, Weisberg SP, et al. Longitudinal profiling of respiratory and systemic immune responses reveals myeloid cell-driven lung inflammation in severe COVID-19. *Immunity.* 2021;54(4):797-814 e6.
27. Larson-Casey JL, Gu L, Fiehn O, and Carter AB. Cadmium-mediated lung injury is exacerbated by the persistence of classically activated macrophages. *J Biol Chem.* 2020;295(46):15754-66.
28. Jiang C, Ting AT, and Seed B. PPAR-gamma agonists inhibit production of monocyte inflammatory cytokines. *Nature.* 1998;391(6662):82-6.

29. Odegaard JI, Ricardo-Gonzalez RR, Goforth MH, Morel CR, Subramanian V, Mukundan L, et al. Macrophage-specific PPARgamma controls alternative activation and improves insulin resistance. *Nature.* 2007;447(7148):1116-20.
30. Camp HS, and Tafuri SR. Regulation of peroxisome proliferator-activated receptor gamma activity by mitogen-activated protein kinase. *J Biol Chem.* 1997;272(16):10811-6.
31. Lee PJ, Zhang X, Shan P, Ma B, Lee CG, Homer RJ, et al. ERK1/2 mitogen-activated protein kinase selectively mediates IL-13-induced lung inflammation and remodeling in vivo. *J Clin Invest.* 2006;116(1):163-73.
32. Hauser S, Adelmant G, Sarraf P, Wright HM, Mueller E, and Spiegelman BM. Degradation of the peroxisome proliferator-activated receptor gamma is linked to ligand-dependent activation. *J Biol Chem.* 2000;275(24):18527-33.
33. Carter AB, and Hunninghake GW. A constitutive active MEK --> ERK pathway negatively regulates NF-kappa B-dependent gene expression by modulating TATA-binding protein phosphorylation. *J Biol Chem.* 2000;275(36):27858-64.
34. Hu E, Kim JB, Sarraf P, and Spiegelman BM. Inhibition of adipogenesis through MAP kinase-mediated phosphorylation of PPARgamma. *Science.* 1996;274(5295):2100-3.
35. Zhu L, Yang T, Li L, Sun L, Hou Y, Hu X, et al. TSC1 controls macrophage polarization to prevent inflammatory disease. *Nat Commun.* 2014;5(1):4696.
36. Garg M, Johri S, Sagar S, Mundhada A, Agrawal A, Ray P, et al. Cardiolipin-mediated PPARgamma S112 phosphorylation impairs IL-10 production and inflammation resolution during bacterial pneumonia. *Cell Rep.* 2021;34(6):108736.
37. Chakraborty K, Raundhal M, Chen BB, Morse C, Tyurina YY, Khare A, et al. The mito-DAMP cardiolipin blocks IL-10 production causing persistent inflammation during bacterial pneumonia. *Nat Commun.* 2017;8(1):13944.
38. Sullivan RJ, Infante JR, Janku F, Wong DJL, Sosman JA, Keedy V, et al. First-in-Class ERK1/2 Inhibitor Ulixertinib (BVD-523) in Patients with MAPK Mutant Advanced Solid Tumors: Results of a Phase I Dose-Escalation and Expansion Study. *Cancer Discov.* 2018;8(2):184-95.
39. Dominici F, Peng RD, Bell ML, Pham L, McDermott A, Zeger SL, et al. Fine particulate air pollution and hospital admission for cardiovascular and respiratory diseases. *JAMA.* 2006;295(10):1127-34.
40. Di Q, Wang Y, Zanobetti A, Wang Y, Koutrakis P, Choirat C, et al. Air Pollution and Mortality in the Medicare Population. *N Engl J Med.* 2017;376(26):2513-22.
41. Rice MB, Ljungman PL, Wilker EH, Dorans KS, Gold DR, Schwartz J, et al. Long-term exposure to traffic emissions and fine particulate matter and lung function decline in the Framingham heart study. *Am J Respir Crit Care Med.* 2015;191(6):656-64.
42. Bowe B, Xie Y, Yan Y, and Al-Aly Z. Burden of Cause-Specific Mortality Associated With PM2.5 Air Pollution in the United States. *JAMA Netw Open.* 2019;2(11):e1915834.
43. Pastuszka JS, Rogula-Kozlowska W, and Zajusz-Zubek E. Characterization of PM10 and PM2.5 and associated heavy metals at the crossroads and urban background site in Zabrze, Upper Silesia, Poland, during the smog episodes. *Environ Monit Assess.* 2010;168(1-4):613-27.
44. Wu Y, Yang X, Wang H, Jia G, and Wang T. Relationship between ambient PM(2.5) exposure and blood cadmium level in children under 14 years in Beijing, China. *J Hazard Mater.* 2021;403:123871.

45. Larson-Casey JL, Vaid M, Gu L, He C, Cai GQ, Ding Q, et al. Increased flux through the mevalonate pathway mediates fibrotic repair without injury. *J Clin Invest.* 2019;129(11):4962-78.
46. Aran D, Looney AP, Liu L, Wu E, Fong V, Hsu A, et al. Reference-based analysis of lung single-cell sequencing reveals a transitional profibrotic macrophage. *Nat Immunol.* 2019;20(2):163-72.
47. Gangwar RS, Vinayachandran V, Rengasamy P, Chan R, Park B, Diamond-Zaluski R, et al. Differential contribution of bone marrow-derived infiltrating monocytes and resident macrophages to persistent lung inflammation in chronic air pollution exposure. *Sci Rep.* 2020;10(1):14348.
48. Xavier MN, Winter MG, Spees AM, den Hartigh AB, Nguyen K, Roux CM, et al. PPARgamma-mediated increase in glucose availability sustains chronic Brucella abortus infection in alternatively activated macrophages. *Cell Host Microbe.* 2013;14(2):159-70.
49. Abdullah Z, Geiger S, Nino-Castro A, Bottcher JP, Muraliv E, Gaidt M, et al. Lack of PPARgamma in myeloid cells confers resistance to Listeria monocytogenes infection. *PLoS One.* 2012;7(5):e37349.
50. Eisele NA, Ruby T, Jacobson A, Manzanillo PS, Cox JS, Lam L, et al. Salmonella require the fatty acid regulator PPARdelta for the establishment of a metabolic environment essential for long-term persistence. *Cell Host Microbe.* 2013;14(2):171-82.
51. Banks AS, McAllister FE, Camporez JP, Zushin PJ, Jurczak MJ, Laznik-Bogoslavski D, et al. An ERK/Cdk5 axis controls the diabetogenic actions of PPARgamma. *Nature.* 2015;517(7534):391-5.
52. Schuh K, and Pahl A. Inhibition of the MAP kinase ERK protects from lipopolysaccharide-induced lung injury. *Biochem Pharmacol.* 2009;77(12):1827-34.
53. Thurlow LR, Joshi GS, and Richardson AR. Peroxisome Proliferator-Activated Receptor gamma Is Essential for the Resolution of Staphylococcus aureus Skin Infections. *Cell Host Microbe.* 2018;24(2):261-70 e4.
54. Nesto RW, Bell D, Bonow RO, Fonseca V, Grundy SM, Horton ES, et al. Thiazolidinedione use, fluid retention, and congestive heart failure: a consensus statement from the American Heart Association and American Diabetes Association. October 7, 2003. *Circulation.* 2003;108(23):2941-8.
55. Dumitru CD, Ceci JD, Tsatsanis C, Kontoyiannis D, Stamatakis K, Lin JH, et al. TNF-alpha induction by LPS is regulated posttranscriptionally via a Tpl2/ERK-dependent pathway. *Cell.* 2000;103(7):1071-83.
56. Ward-Kavanagh LK, Lin WW, Sedy JR, and Ware CF. The TNF Receptor Superfamily in Co-stimulating and Co-inhibitory Responses. *Immunity.* 2016;44(5):1005-19.
57. Parsons PE, Matthay MA, Ware LB, Eisner MD, and National Heart LBIARDSCTN. Elevated plasma levels of soluble TNF receptors are associated with morbidity and mortality in patients with acute lung injury. *Am J Physiol Lung Cell Mol Physiol.* 2005;288(3):L426-31.
58. Larson-Casey JL, Deshane JS, Ryan AJ, Thannickal VJ, and Carter AB. Macrophage Akt1 Kinase-Mediated Mitophagy Modulates Apoptosis Resistance and Pulmonary Fibrosis. *Immunity.* 2016;44(3):582-96.
59. Butler A, Hoffman P, Smibert P, Papalexi E, and Satija R. Integrating single-cell transcriptomic data across different conditions, technologies, and species. *Nat Biotechnol.* 2018;36(5):411-20.

Figures and Legends

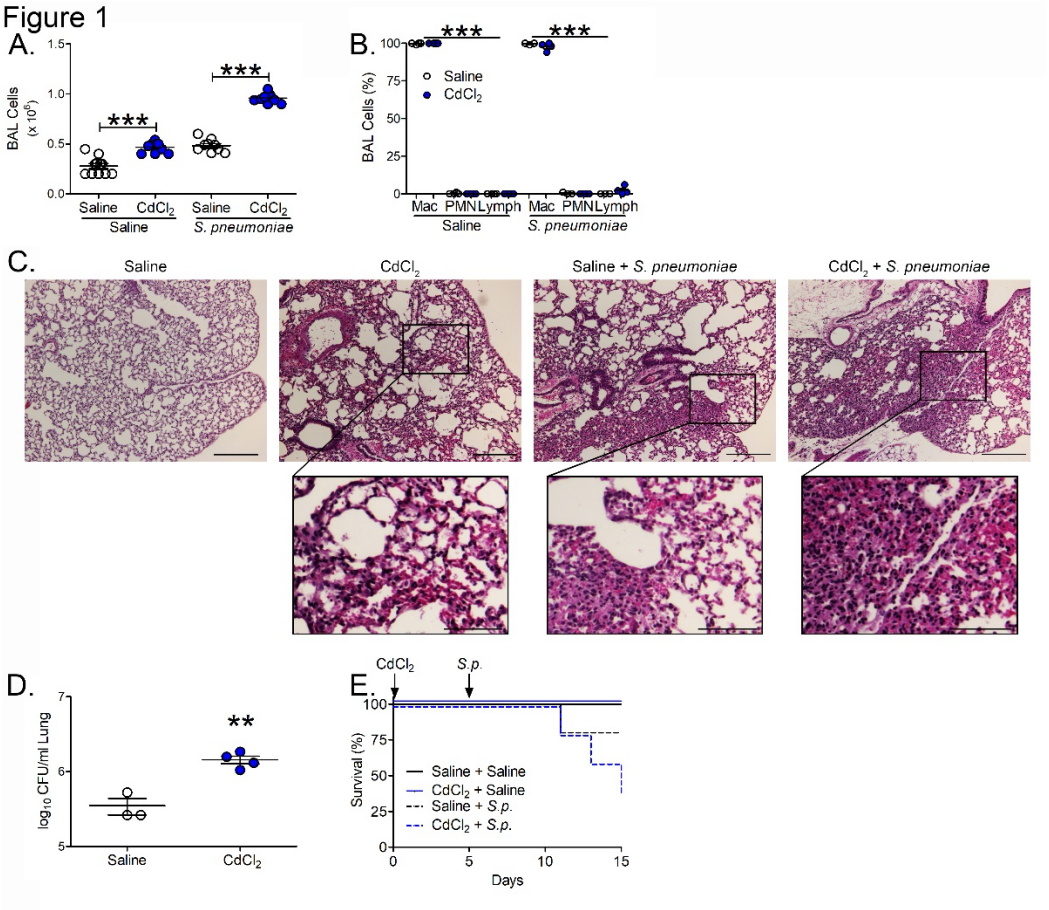

Figure 1. **Cadmium exacerbates lower respiratory tract infections.** WT mice were exposed to saline or $CdCl_2$ (100ng/kg) by i.t. administration. On day 5 mice were exposed to saline or 10^3 *Streptococcus pneumoniae* (strain A66.1, type 3) i.t. and BAL was performed on day 15. (**A**) Number of BAL cells. n = 9-17. (**B**) Cell differential to identify macrophages (mac), neutrophil (PMN), and lymphocytes (lymph). n = 3-5. (**C**) Representative hematoxylin and eosin staining of lung tissues. n = 3-5. Bar = 250 µm; inset bar = 100 µm. (**D**) Lung colony forming units. n = 3-4. (**E**) Kaplan-Meier survival curves. n = 4-5. **, $p < 0.001$; ***, $p < 0.0001$. Values shown as mean ± S.E.M. One-way AVOVA, Tukey's post hoc (**A**, **B**). Student's t-test (**D**).

Figure 2

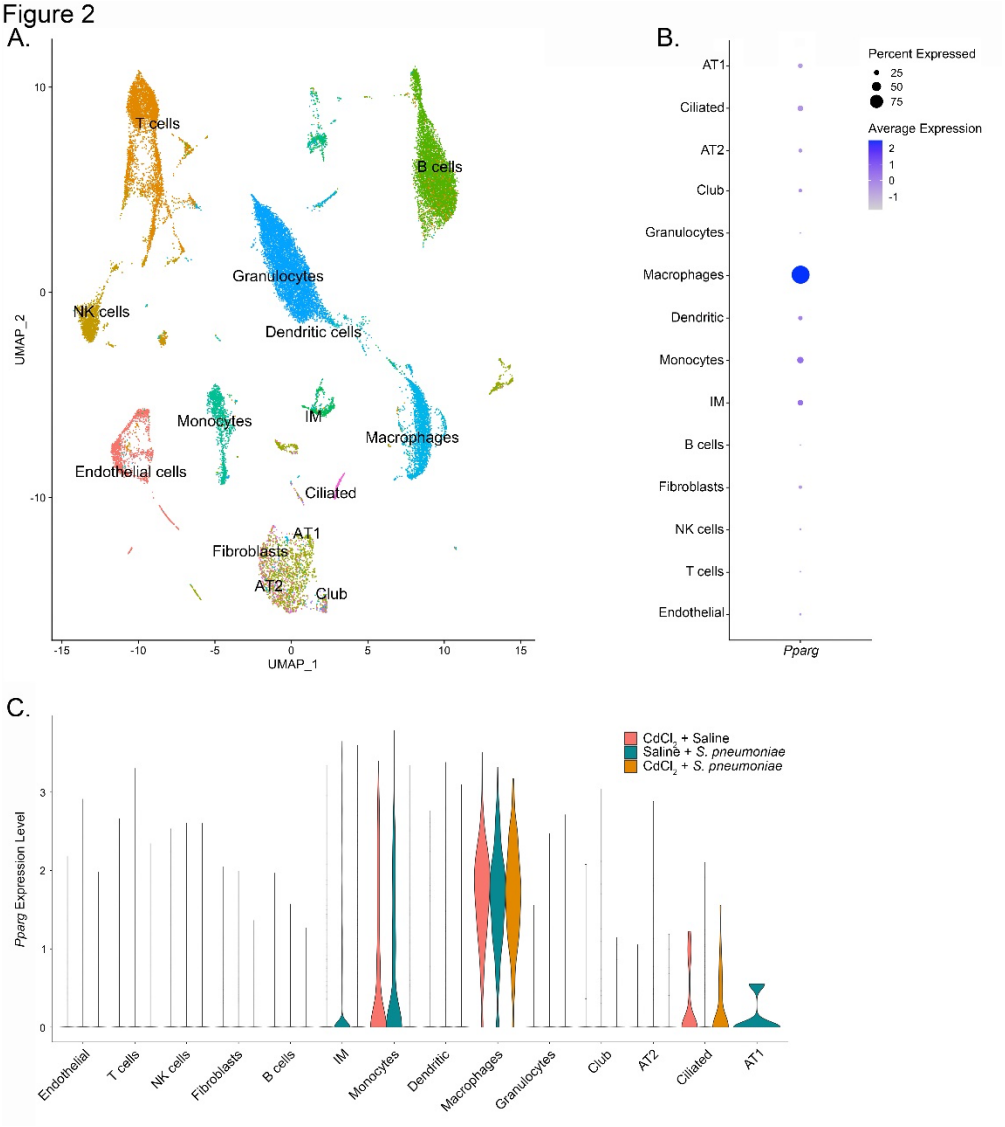

Figure 2. Single cell RNA-sequencing identifies *Pparg* expression in macrophages. WT mice were exposed to saline or $CdCl_2$ by i.t. On day 5 mice were exposed to saline or *S. pneumoniae* i.t. and lungs were harvested on day 15. (**A**) Uniform manifold approximation and projection (UMAP) plot identifying 15 cell clusters by single cell RNA-sequencing (one mouse per condition). (**B**) Dot plot of *Pparg* expression in all cell clusters. (**C**) Violin plot of *Pparg* expression in exposed mice in each cell cluster. Alveolar epithelial type I cell (AT1); alveolar epithelial type II cell (AT2); interstitial macrophages (IM).

Figure 3

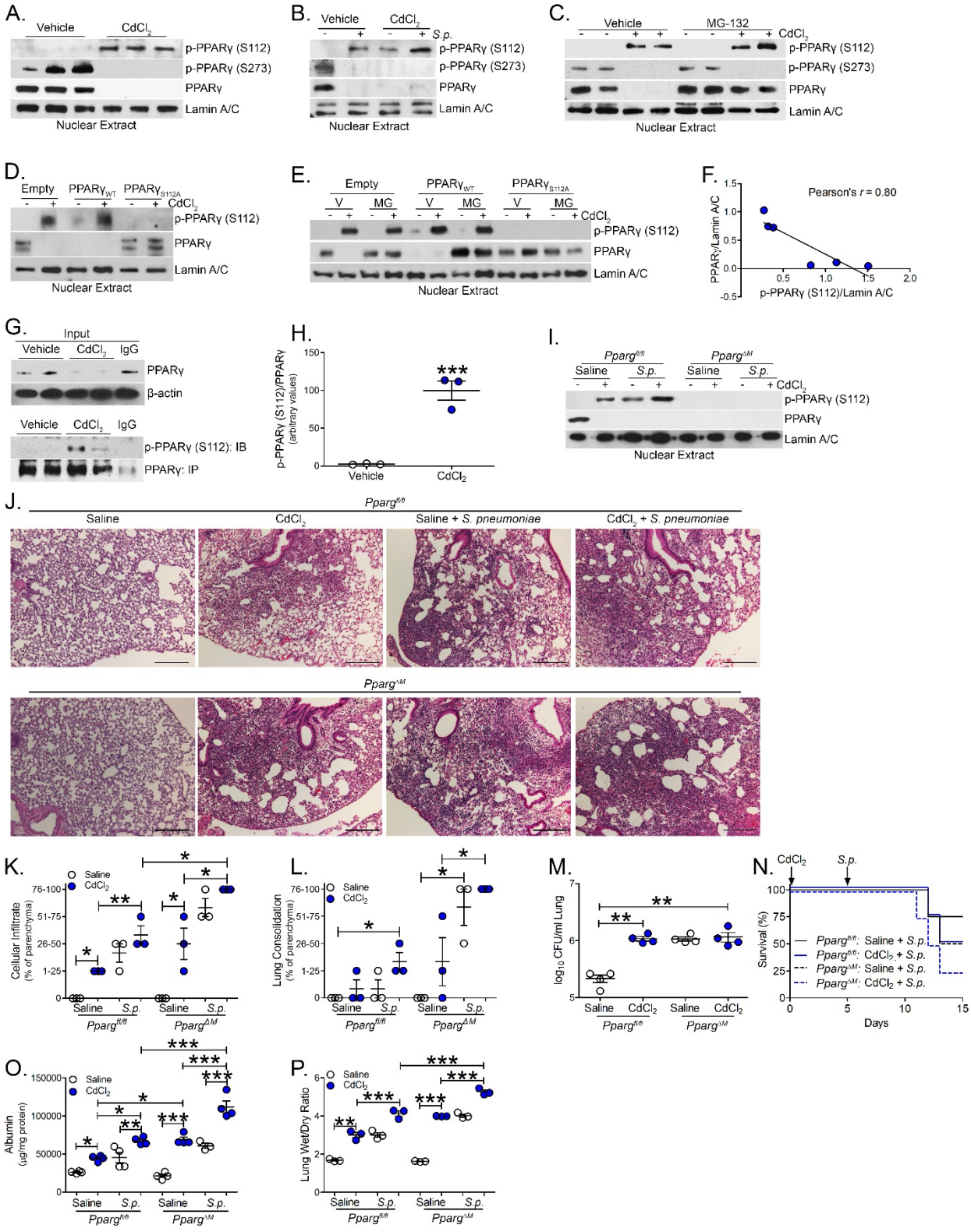
A.
Vehicle
CdCl2
p-PPARγ (S112)
p-PPARγ (S273)
PPARγ
Lamin A/C
Nuclear Extract
B.
Vehicle
CdCl2
S.p.
p-PPARγ (S112)
p-PPARγ (S273)
PPARγ
Lamin A/C
Nuclear Extract
C.
Vehicle
MG-132
CdCl2
p-PPARγ (S112)
p-PPARγ (S273)
PPARγ
Lamin A/C
Nuclear Extract
D.
Empty
PPARγWT
PPARγS112A
CdCl2
p-PPARγ (S112)
PPARγ
Lamin A/C
Nuclear Extract
E.
Empty
PPARγWT
PPARγS112A
V
MG
CdCl2
p-PPARγ (S112)
PPARγ
Lamin A/C
Nuclear Extract
F.
Pearson's r = 0.80
PPARγ/Lamin A/C
p-PPARγ (S112)/Lamin A/C
G.
Input
Vehicle
CdCl2
IgG
PPARγ
β-actin
p-PPARγ (S112): IB
PPARγ: IP
H.
p-PPARγ (S112)/PPARγ (arbitrary values)
Vehicle
CdCl2
I.
Pparg fl/fl
Pparg ΔM
Saline
S.p.
CdCl2
p-PPARγ (S112)
PPARγ
Lamin A/C
Nuclear Extract
J.
Pparg fl/fl
Saline
CdCl2
Saline + S. pneumoniae
CdCl2 + S. pneumoniae
Pparg ΔM
K.
Cellular Infiltrate (% of parenchyma)
Saline
CdCl2
S.p.
Pparg fl/fl
Pparg ΔM
L.
Lung Consolidation (% of parenchyma)
M.
log10 CFU/ml Lung
N.
CdCl2
S.p.
Survival (%)
Days
Pparg fl/fl: Saline + S.p.
Pparg fl/fl: CdCl2 + S.p.
Pparg ΔM: Saline + S.p.
Pparg ΔM: CdCl2 + S.p.
O.
Albumin (μg/mg protein)
P.
Lung Wet/Dry Ratio

Figure 3. Cadmium mediated PPARɣ phosphorylation at Ser^{112} resulting in greater lung injury. (**A**) Nuclear immunoblot analysis of THP-1 cells exposed to $CdCl_2$ (50 μM, 3h). (**B**) Nuclear immunoblot analysis from BAL cells from exposed WT mice. (**C**) Immunoblot analysis in isolated nuclear extract of THP-1 cells treated with vehicle or MG-132 (20 μM, 6h) and saline or $CdCl_2$ (50 μM, 3h). (**D**) Immunoblot analysis in isolated nuclear extract of THP-1 cells expressing empty, $PPAR\gamma_{WT}$, or $PPAR\gamma_{S112A}$ treated with saline or $CdCl_2$. (**E**) Immunoblot analysis in isolated nuclear extract of THP-1 cells expressing empty, $PPAR\gamma_{WT}$, or $PPAR\gamma_{S112A}$ treated with vehicle or MG-132. (**F**) Pearson's correlation of densitometry of phosphorylated PPARɣ (S112) and PPARɣ relative to Lamin A/C in transfected THP-1 cells treated with vehicle in E. (**G**) Immunoprecipitation of PPARɣ from cadmium-exposed THP-1 cells with (**H**) statistical quantification of phosphorylated PPARɣ (S112) relative to PPARɣ in G. (**I**) Nuclear immunoblot analysis of BAL cells from exposed *Pparg*$^{fl/fl}$ and *Pparg*$^{\Delta M}$ mice. (**J**) Representative hematoxylin and eosin staining of lung tissues. n = 3-5. Bar = 250 μm. Scoring of lung tissue from J for (**K**) cellular infiltrate and (**L**) consolidation. (**M**) Lung colony forming units. n = 4. (**N**) Kaplan-Meier survival curves. n = 4-5. (**O**) Albumin levels in BALF. n = 3-4. (**P**) Wet to dry ratio of lung weight from exposed mice. n = 3. *, $p < 0.05$; **, $p < 0.001$; ***, $p < 0.0001$. Values shown as mean ± S.E.M. One-way AVOVA, Tukey's post hoc. Person's coefficient was used for F.

Figure 4

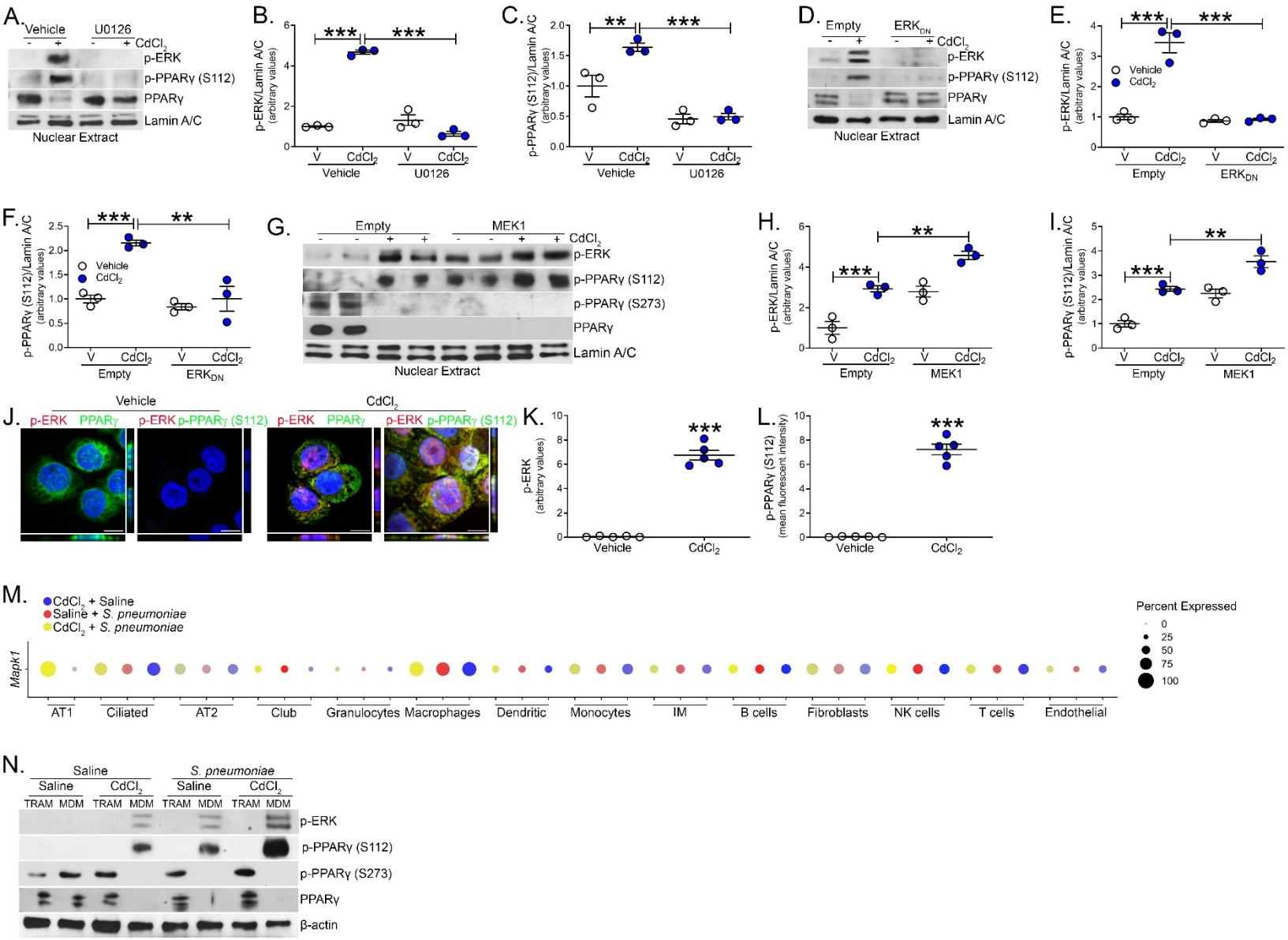
A.
Vehicle
U0126
CdCl2
p-ERK
p-PPARγ (S112)
PPARγ
Lamin A/C
Nuclear Extract
B.
p-ERK/Lamin A/C (arbitrary values)
Vehicle
U0126
C.
p-PPARγ (S112)/Lamin A/C (arbitrary values)
D.
Empty
ERKDN
E.
F.
G.
Empty
MEK1
p-PPARγ (S273)
H.
I.
J.
Vehicle
CdCl2
p-ERK
PPARγ
p-PPARγ (S112)
K.
p-ERK (arbitrary values)
L.
p-PPARγ (S112) (mean fluorescent intensity)
M.
CdCl2 + Saline
Saline + S. pneumoniae
CdCl2 + S. pneumoniae
Mapk1
Percent Expressed
AT1
Ciliated
AT2
Club
Granulocytes
Macrophages
Dendritic
Monocytes
IM
B cells
Fibroblasts
NK cells
T cells
Endothelial
N.
Saline
S. pneumoniae
TRAM
MDM
β-actin

Figure 4. ERK activation mediates phosphorylation of PPARɣ. (**A**) Nuclear immunoblot analysis of THP-1 cells exposed to vehicle or U0126 (10 μM, 1h) and $CdCl_2$ (50 μM, 3h) with statistical quantification of (**B**) p-ERK and (**C**) p-PPARɣ (S112) *n* = 3. (**D**) Nuclear immunoblot analysis of THP-1 cells transfected with empty or ERK_{DN} and exposed to saline or $CdCl_2$ with statistical quantification of (**E**) p-ERK and (**F**) p-PPARɣ (S112) *n* = 3. (**G**) Nuclear immunoblot analysis of THP-1 cells transfected with empty or MEK1 and exposed to saline or $CdCl_2$ with statistical quantification of (**H**) p-ERK and (**I**) p-PPARɣ (S112) *n* = 3. (**J**) Representative confocal imaging of exposed MH-S cells. Bar = 10 μm. Statistical quantification of (**K**) p-ERK and (**L**) p-PPARɣ (S112) staining *n* = 5. (**M**) Dot plot of percent expressed of *Mapk1* expression in each cell cluster in exposed mice from lung tissue subjected to scRNA-seq. (**N**) Immunoblot analysis of FACS-sorted BAL cells from exposed WT mice. Tissue resident alveolar macrophages (TRAM, $CD45^{+}CD11b^{+/-}Ly6G^{-}CD64^{+}Ly6C^{-}$Siglec F^{hi}) and monocyte-derived macrophages (MDM, $CD45^{+}CD11b^{+/-}Ly6G^{-}CD64^{+}Ly6C^{-}$Siglec F^{low}). **, $p < 0.001$; ***, $p < 0.0001$. Values shown as mean ± S.E.M. Student's *t*-test used in K-L. One-way AVOVA, Tukey's post hoc.

Figure 5

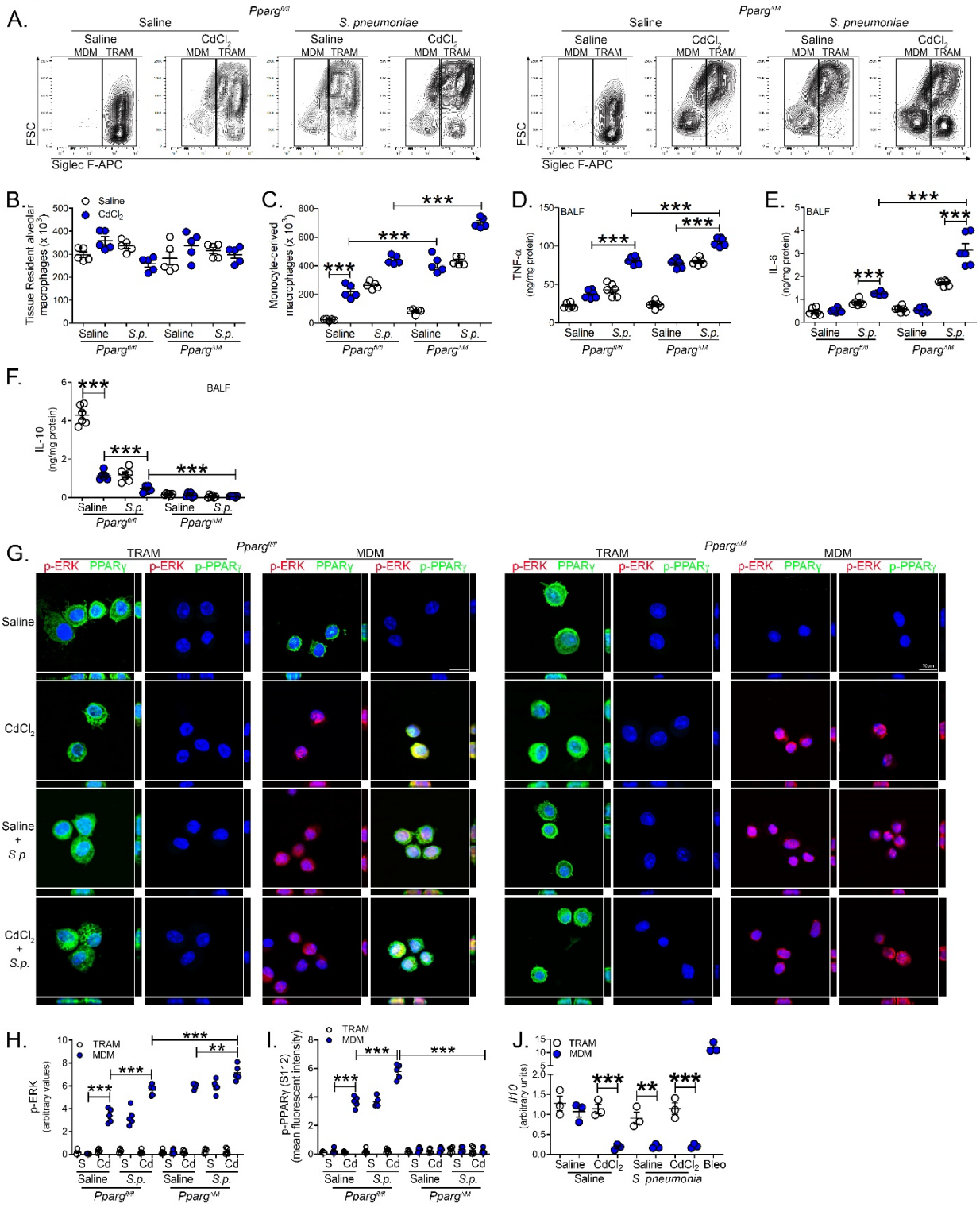
A.
Pparg^fl/fl
Pparg^ΔM
Saline
S. pneumoniae
Saline
CdCl2
MDM TRAM
FSC
Siglec F-APC
B.
Tissue Resident alveolar macrophages (x 10^3)
C.
Monocyte-derived macrophages (x 10^3)
D.
BALF
TNF-α (ng/mg protein)
E.
BALF
IL-6 (ng/mg protein)
F.
BALF
IL-10 (ng/mg protein)
G.
TRAM
MDM
p-ERK PPARγ p-ERK p-PPARγ
Saline
CdCl2
Saline + S.p.
CdCl2 + S.p.
H.
p-ERK (arbitrary values)
I.
p-PPARγ (S112) (mean fluorescent intensity)
J.
Il10 (arbitrary units)
Saline
CdCl2
Bleo
S. pneumonia
S.p.
***
**

Figure 5. Severe LRTIs inhibit PPARɣ expression in monocyte-derived macrophages. (**A**) Representative flow cytometry plots of tissue resident alveolar macrophages (TRAM, $CD45^{+}CD11b^{+/-}Ly6G^{-}CD64^{+}Ly6c^{-}$Siglec F^{hi}) and monocyte-derived macrophages (MDM, $CD45^{+}CD11b^{+/-}Ly6G^{-}CD64^{+}Ly6c^{-}$Siglec F^{low}) from exposed *PPARɣ*$^{fl/fl}$ and *PPARɣ*$^{-/-}$*Lyz2-cre* mice on day 15. Number of (**B**) TRAMs and (**C**) MDMs in BAL. $n = 5$. (**D**) TNF-α, (**E**) IL-6, and (**F**) IL-10 levels in BALF. $n = 6$. (**G**) Representative confocal imaging of FACS-sorted BAL cells. $n = 3$. Bar = 10 μm. Statistical quantification of confocal imaging of (**H**) p-ERK and (**I**) p-PPARɣ (S112) staining $n = 5$. (**J**) IL-10 mRNA expression in FACS-sorted BAL cells. $n = 3$. ** $p < 0.001$; ***, $p < 0.0001$. Values shown as mean ± S.E.M. One-way AVOVA, Tukey's post hoc.

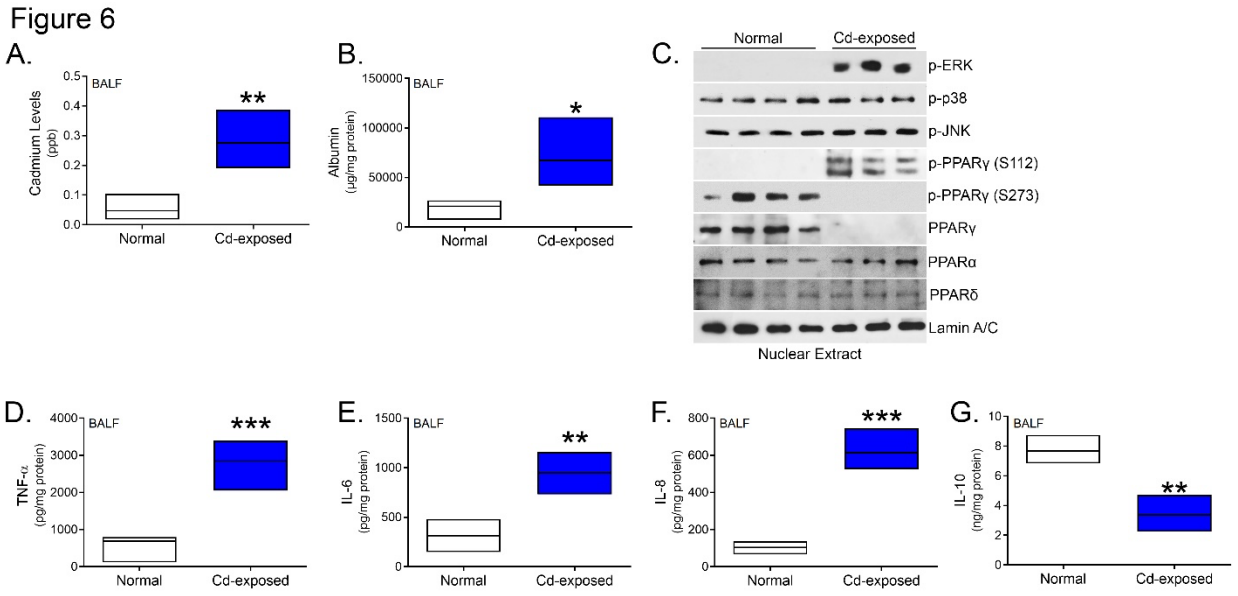

Figure 6. Subjects residing in areas with high air cadmium levels show PPARɣ inhibition. (**A**) BAL fluid samples from control and cadmium-exposed subjects were subjected to inductively coupled plasma mass spectrometry to determine cadmium. n = 3-4. (**B**) Albumin levels in BAL fluid from control and cadmium-exposed subjects. n = 3-4. (**C**) Nuclear immunoblot from BAL cells from normal and cadmium-exposed subjects. Levels of in (**D**) TNF-α, (**E**) IL-6, (**F**) IL-8, and (**G**) IL-10 in BALF. n = 3-4. * $p < 0.05$; ** $p < 0.001$; *** $p < 0.0001$. Values shown as mean ± S.E.M. Student's t-test.

Figure 7

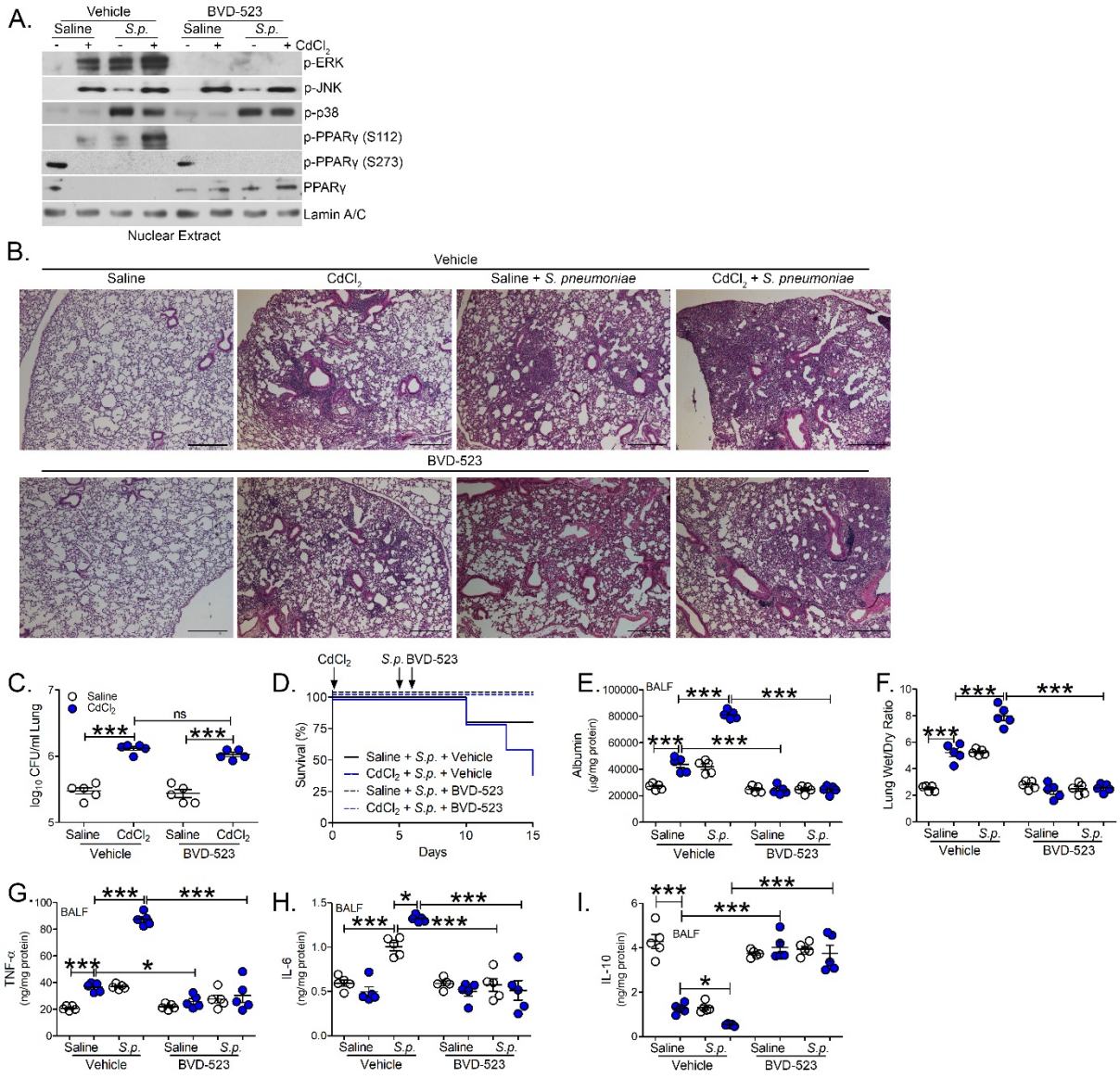

Figure 7. Inhibition of ERK activation reduces lung injury facilitating PPARg activation during LRTI. WT mice were exposed to saline or $CdCl_2$ (100ng/kg) by i.t. administration. On day 5 mice were exposed to saline or 10^3 *Streptococcus pneumoniae* (strain A66.1, type 3) i.t. Vehicle or BVD-523 (8.6 mg/kg) was administered twice daily to mice at day 6 until day 15. BAL was performed on day 15. (**A**) Nuclear immunoblot analysis from BAL cells from exposed mice. (**B**) Representative hematoxylin and eosin staining of lung tissues. $n = 5$. Bar = 250 μm. (**C**) Lung

colony forming units. $n = 5$. (**D**) Kaplan-Meier survival curves. $n = 5$. (**E**) Albumin levels in BALF. $n = 5$. (**F**) Wet to dry ratio of lung weight from exposed mice. $n = 5$. (**G**) TNF-α, (**H**) IL-6, and (**I**) IL-10 levels in BALF. $n = 5$. *, $p < 0.05$; ***, $p < 0.0001$. Values shown as mean ± S.E.M. One-way AVOVA, Tukey's post hoc.